

## Solid N<sub>2</sub> and CO in nanoporous glasses

P. Huber, D. Wallacher, and K. Knorr

*Technische Physik, Universität des Saarlandes, D-66041 Saarbrücken, Germany*

(Received 7 April 1999)

N<sub>2</sub> and CO condensed into nanoporous glasses have been investigated by vapor pressure measurements and x-ray diffraction as a function of temperature and fractional filling. The pore material is stable with respect to bulk condensation for any fractional filling. The adsorbate on the pore walls has to be distinguished from the capillary condensate in the center of the pores. This distinction can be made not only in the liquid, but also in the solid state. The solid capillary condensate is quasi-hcp at higher temperatures. N<sub>2</sub> remains in this state down to the lowest temperatures, even in pores as large as 130 Å diameter, whereas CO transforms into the orientationally ordered *Pa3* phase. On heating an orientationally disordered intermediate phase with a fcc center-of-mass lattice is observed. [S0163-1829(99)08941-9]

### I. INTRODUCTION

When materials are confined within small pores in the range of a few nm, their properties may be substantially modified with respect to the bulk state. It is, e.g., well known that the melting temperature is significantly reduced in such pores.<sup>1,2</sup> Considerable effort has been spent on understanding the liquid state of pore condensed systems,<sup>3,4</sup> but there are only a few investigations of the solid state.

Recently, we have reported on the structure, thermodynamics, and melting of pore condensed Ar.<sup>5</sup> The present study deals with N<sub>2</sub> and CO, nonspherical molecules which have orientational degrees of freedom. The major objective is insight into the effects of the confinement on a structural phase transition, namely, the  $\alpha$ - $\beta$  transition. N<sub>2</sub> and CO are molecules of similar size and shape. As bulk systems, they have closely related structural and thermodynamic properties: see Table I. The melting temperature and entropy of melting are almost equal. Bulk N<sub>2</sub> and CO are isomorphous in both solid phases. The high-temperature  $\beta$  phase is hcp with a practically ideal *c/a* ratio. Here the molecules are orientationally disordered due to rapid reorientations. At lower temperatures the bulk solids undergo a first-order phase transition into the  $\alpha$  phase (cubic, *Pa3*), which involves a change of the center-of-mass lattice from the hcp-stacking sequence *AB...* to the fcc-stacking sequence *ABC...* and an orientational ordering of the molecular axes, i.e., of the quadrupole moments, such that each of the four

TABLE I. Thermodynamic data of N<sub>2</sub> and CO (Ref. 19);  $T_3^{\text{bulk}}$ , triple-point temperature;  $T_{\alpha\beta}$ ,  $\alpha$ - $\beta$  phase transition temperature;  $\Delta S_m$ , entropy of melting;  $\Delta S_{\alpha\beta}$ , entropy change at the  $\alpha$ - $\beta$  transition;  $Q$ , quadrupole moment;  $d$ , dipole moment.

	N <sub>2</sub>	CO
$T_3^{\text{bulk}}$ (K)	63.15	68.9
$T_{\alpha\beta}$ (K)	35.61	61.55
$\Delta S_m$ (J/mol/K)	11.43	12.27
$\Delta S_{\alpha\beta}$ (J/mol/K)	6.446	10.30
$Q$ (cgs units)	$-1.4 \times 10^{-26}$	$-2.5 \times 10^{-26}$
$d$ (D)		0.12

molecules of the cell points along one of the four  $\langle 111 \rangle$  directions.<sup>6,7</sup> However, the entropy change at the  $\alpha$ - $\beta$  transition of N<sub>2</sub> is only 63% of that of CO. Furthermore,  $\beta$ -N<sub>2</sub> is stable over a much wider temperature interval than  $\beta$ -CO; see Table I. In short, properties that depend on the spherical average of the intermolecular interactions, such as melting, are similar; the properties that depend on the anisotropic part of the intermolecular interactions ( $T_{\alpha\beta}, \Delta S_{\alpha\beta}$ ) show pronounced differences. The small dipole moment of CO appears to have no effect on the structure.

Our first x-ray diffraction patterns on solid N<sub>2</sub> confined in a porous glass with an average pore diameter of 50 Å showed that this sample remained hcp (with a lot of stacking faults) down to the lowest temperatures.<sup>8</sup> Here we present additional measurements on N<sub>2</sub> in pores with 25, 75, and 130 Å as well as investigations of pore condensed CO in pores with 75 Å diameter.

### II. EXPERIMENT

The experimental setup allows the simultaneous measurement of volumetric adsorption isotherms and x-ray diffraction patterns ( $\lambda = 1.542$  Å). Details have been provided elsewhere.<sup>5</sup> The thermodynamic state of the pore condensed material will be given in terms of the variables temperature  $T$ , reduced vapor pressure  $p = p/p_{\text{sat}}$ , and filling fraction  $f = N/N_0$ ;  $p_{\text{sat}}(T)$  is the saturated vapor pressure of the bulk.  $N$  is the number of molecules in the sample cell,  $N_0$  the number necessary for the complete filling of the pores.  $N_0$  is about 10 mmol.

The matrix materials used in our study are two controlled pore glasses, xerogels ‘‘Gelsil’’ with nominal pore diameters of 25 and 75 Å as specified by the manufacturer (Geltech Inc. Orlando, FL) and a Vycor glass with a pore diameter of 130 Å. The porous glasses have been checked by routine characterization in form of N<sub>2</sub> adsorption-desorption isotherms at 77 K based on the Brunauer-Emmett-Teller (B.E.T.) analysis for the initial part of the isotherm and on the Kelvin equation for the vapor pressure necessary for emptying the pores.<sup>9</sup>

Some results have been obtained by adsorption and desorption at constant temperatures, most, however, by cooling

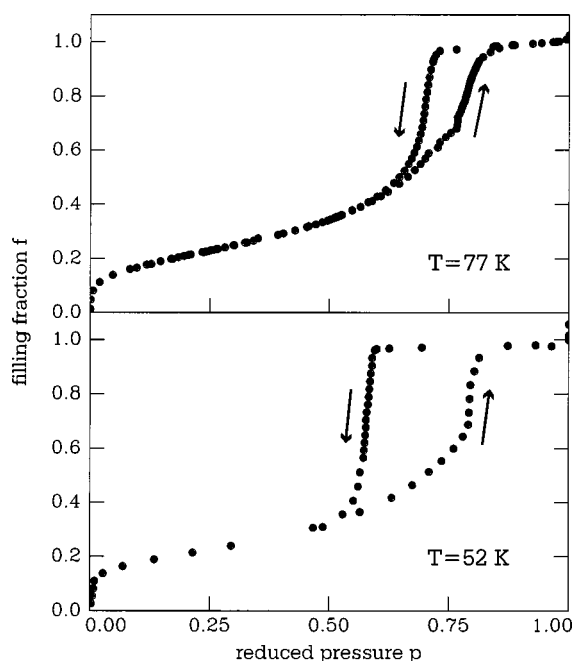


FIG. 1. Adsorption-desorption isotherms of N<sub>2</sub> in a 75 Å controlled pore glass (“Gelsil”) in the liquid state at 77 K and in the solid state at 52 K.

and heating with approximately constant filling fractions. Such “quasi-isosteric” experiments are adequate at higher temperatures where the pore condensate is in equilibrium with its vapor at sufficiently large vapor pressures. Problems arise at lower  $T$ , in our experiment below about 45 K, because of an extremely slow equilibration of the vapor pressure. See the discussion in Ref. 5. Below 50 K some mbar of He contact gas have been added into the cell.

### III. RESULTS AND DISCUSSION

#### A. Nitrogen

The 77 K adsorption-desorption isotherm  $f$  as function of  $p$  for the 75 Å xerogel is shown in Fig. 1. It has been recorded by adding consecutively small amounts of gas into the cell and by allowing the pressure to relax toward the equilibrium value in each step. At this temperature the equilibration time is several minutes.

The general shape of the isotherm including the hysteric part can be understood in terms of adsorption and capillary condensation of liquids in cylindrical pores.<sup>3</sup> The initial part of the isotherm is similar to what is obtained for physisorption on planar heterogeneous substrates. For low fractional fillings  $f$ , the N<sub>2</sub> molecules form a thin adsorbate film on the pore walls. Owing to their amorphous state of the matrix, the walls have to be regarded as a heterogeneous substrate for adsorption. A quantitative analysis shows that the low- $f$  part of the isotherm is reasonably well described by the B.E.T. model. The resulting parameters are the specific surface area of 560 m<sup>2</sup>/g and the B.E.T. heat of adsorption of 660 cal/mol.<sup>9</sup> Here we assumed an area per molecule of 16.2 Å<sup>2</sup>. At higher  $f$ , at a characteristic pressure  $p_d$ , as defined experimentally from the point of steepest ascent, a first-order phase transition into the capillary condensed state occurs. The transition is accompanied by hysteresis with respect to adsorp-

tion and desorption. See our work on Ar for a discussion of this transition and its connection with the melting transition. The capillary condensate in the center of the pores empties on desorption at a characteristic pressure  $p_d$ , leaving behind an adsorbate film on the pore walls. Following density functional calculations we will assume that  $p_d$  (and not  $p_a$ ) is the equilibrium vapor pressure of the capillary condensate.<sup>10</sup>

The lower panel of Fig. 1 shows the adsorption-desorption isotherm of N<sub>2</sub> at  $T=52$  K. Here the pore filling is solid (see the diffraction patterns of Fig. 3). The equilibration time of the vapor pressure at higher  $f$  is several hours.

The general shape of the 52 K isotherm is similar to that of the liquid state. The initial parts of the isotherms at  $T=77$  and 52 K are in fact identical. However, the adsorption branch of the hysteric region is much steeper,  $p_d$  is lower, and the hysteresis loop is wider than in the liquid state. In summary, the isotherms of Fig. 1 show that the pore filling is stable with respect to the condensation of the bulk, both in the liquid and solid regimes, that the adsorbate state at low  $f$  is practically  $T$  independent, and that not only in the liquid, but also in the solid state the pores can be filled via a first-order phase transition, namely, capillary condensation.

Figure 2 shows diffraction patterns of solid N<sub>2</sub> in several types of porous glass for almost complete filling. Note that the contribution of the substrate to the diffraction pattern has been subtracted, properly accounting for the  $f$ -dependent absorption of x rays. The figure also includes diffraction patterns of the two phases of bulk N<sub>2</sub> which have been prepared by evaporation onto the external surface of the porous glass sample. The diffraction patterns of the solid confined in pores of different size show little  $T$  dependence: see Fig. 2 for  $T=20$  K. Thus one can rule out a structural phase transition within the solid state down to 16 K, the lowest temperature investigated. The widths of the reflections increase with decreasing pore diameter. The diffraction pattern obtained for the smallest pores, with a diameter  $D=25$  Å, is of the type which is typical for an amorphous structure. The patterns for pores with  $D=130$  and 75 Å are very similar. They show five Bragg peaks, which all coincide with reflections of bulk hcp  $\beta$ -N<sub>2</sub>, although with altered intensity ratios and enhanced linewidths. The (102) reflection is missing: the (103) reflection is extremely broadened, but can be still identified. Analogous observations have been made in neutron diffraction studies on H<sub>2</sub> and D<sub>2</sub> in Vycor glass,<sup>11,12</sup> where in fact the similarity to a hcp pattern was even lesser. Recently, we have shown that the differences between the bulk hcp diffraction pattern and the diffraction pattern of the confined solid N<sub>2</sub> in 50 Å pores can be reasonably well explained by finite size and stacking faults.<sup>6</sup> This concept also holds for solid N<sub>2</sub> confined in the somewhat larger pores of 75 and 130 Å of the present study. Here we arrive at stacking fault probabilities around 0.3 for both diameters and the crystallite sizes  $L$  given in Table II as derived from the linewidths of four powder lines by means of the Scherrer formula.  $L$  exceeds the pore diameter. Obviously, the confined solid can develop crystalline coherence along the pores over quite a distance. The largest value of  $L$  is obtained from the width of the (002) reflection, suggesting that maximum coherence is obtained for crystallites which are grown in an orientation such that the  $c$  axis is parallel to the pore axis.

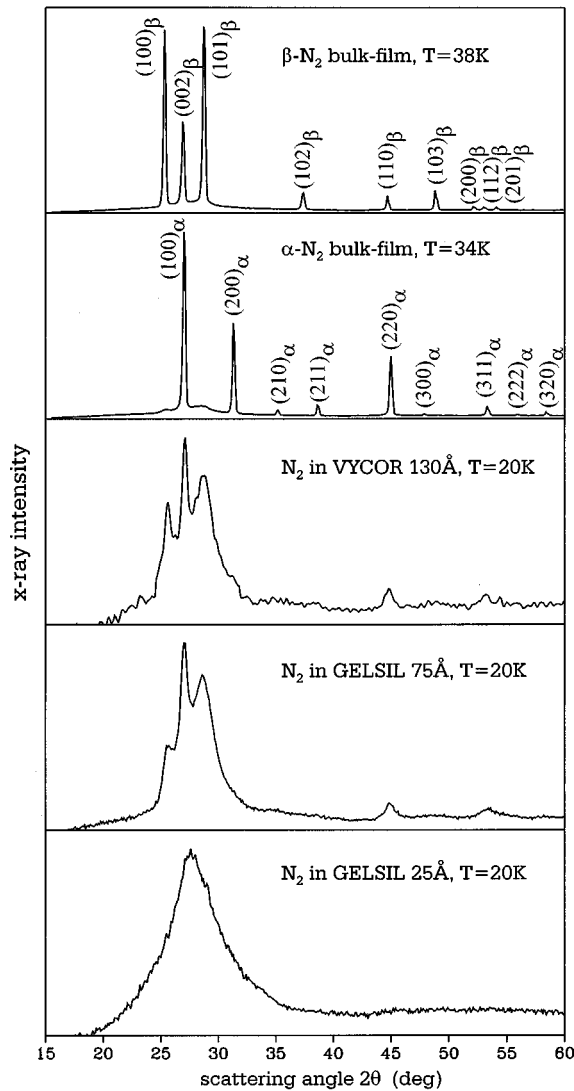


FIG. 2. Diffraction patterns of a bulk  $N_2$  film below and above  $T_{\alpha\beta}^{\text{bulk}}$  and of  $N_2$  confined in porous glasses with various pore diameters. All patterns are for practically completely filled pores at  $T = 20$  K.

Figure 3 shows the most significant part of the diffraction pattern for pores with a diameter  $D$  of  $75 \text{ \AA}$  on cooling and heating through the liquid-solid transition. Solidification, indicated by the appearance of the (100), (002), and (101) hcp Bragg peaks, occurs at about  $T_S = 54$  K, melting at about  $T_m = 58$  K. Thus there is a thermal hysteresis of about 4 K. For the pore diameters of 130 and  $25 \text{ \AA}$ ,  $T_S$  is 58 and 47 K

TABLE II. The coherence length  $L$  calculated from the width of the reflections ( $hkl$ ) for  $N_2$  in pores with different diameters  $D$ .

( $hkl$ )	$L$ ( $\text{\AA}$ )	$D$ ( $\text{\AA}$ )
(100)	181	
(110)	119	75
(002)	274	
(100)	201	
(110)	159	130
(002)	450	

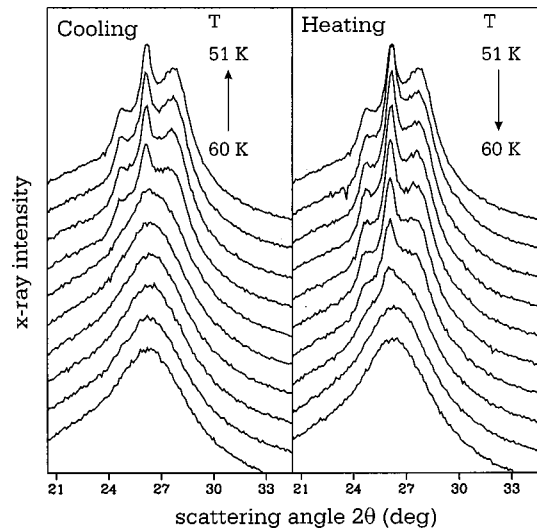


FIG. 3. Diffraction patterns of  $N_2$  confined in a  $75 \text{ \AA}$  controlled pore glass taken in temperature steps of 1 K on cooling and heating through the temperature range of melting.

and  $T_m$  is 61 and 49 K, respectively. The relative shift  $\delta = 1 - T_m/T_3^{\text{bulk}}$  of the melting temperature relative to the triple point of the bulk system is approximately proportional to the inverse pore diameter,  $1/D$ . Analogous observations have been made in many types of material in confined geometries, ranging from small molecules to organic chain molecules and metals.<sup>13-15</sup> The proportionality of  $\delta$  and  $1/D$  stems from the competition of a surface and a volume energy, and is thus of simple geometric origin and of little help for discriminating between different models.<sup>16</sup> In our recent work on confined Ar we have worked out the connection of  $T_S$  and  $T_m$  with the difference of the chemical potential of the pore and bulk condensates.

Figure 4 shows diffraction patterns as a function of filling,  $0.21 < f < 0.94$ , which have been recorded in connection with adsorption steps of the 52 K isotherm of Fig. 1. For  $f < 0.73$  the diffraction patterns have a broad maximum at about  $2\Theta = 27^\circ$  and a second weak and even broader one around  $48^\circ$ . These patterns are characteristic of the highly disordered, amorphous structure of the adsorbate state of the initial part of the isotherms. A comparison to adsorbed monolayers on planar homogeneous substrates gives further insight into these structures.  $N_2$  monolayers on graphite (001) form a two-dimensional triangular center-of-mass lattice.<sup>17</sup> We have calculated the powder diffraction pattern of such a lattice for different sample sizes  $L$  and arrive at an acceptable description of the low- $f$  patterns by choosing values of  $L$  of the order of  $20 \text{ \AA}$ : see Fig. 5 for  $f = 0.11$ . The first maximum is identified as the (10) peak; the second is due to the strongly broadened, overlapping (11) and (20) reflections of the triangular lattice. The resulting next-neighbor distance is  $4.1 \text{ \AA}$ . This is close to the distance in the orientationally disordered hcp  $\beta$  phase of bulk  $N_2$ . Hence we think that the  $N_2$  molecules of the adsorbed layer on the pore walls are randomly oriented. The resulting area per molecule is  $14.5 \text{ \AA}^2$ , significantly smaller than the value of  $16.2 \text{ \AA}^2$  which is usually chosen for the B.E.T. analysis of the surface area.<sup>18</sup>

For  $f$  up to a value of 0.65, the diffraction pattern does not change much, apart from an increase of the diffracted inten-

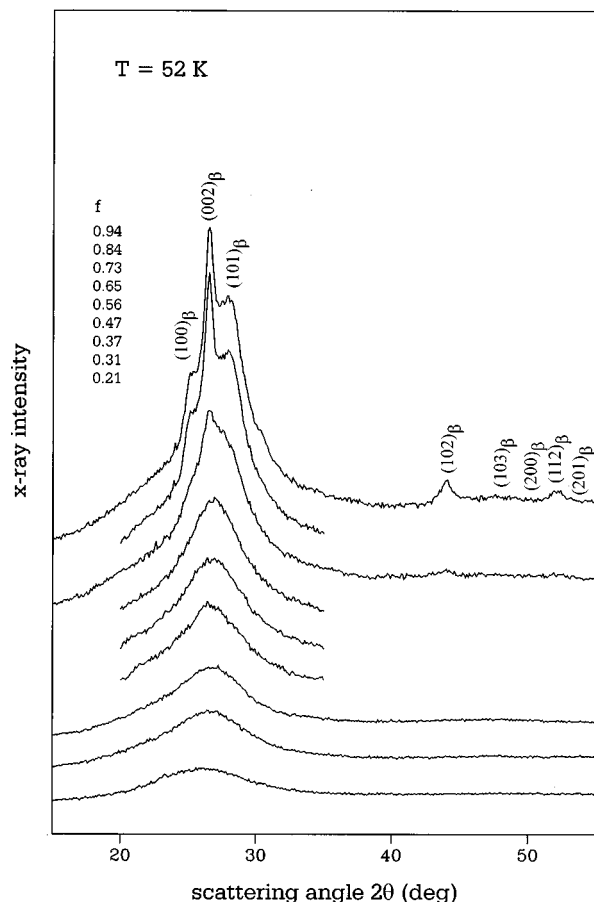


FIG. 4. The diffraction pattern of the solid state of N<sub>2</sub> ( $T = 52$  K) in  $75 \text{ \AA}$  pores as a function of fractional filling  $f$ .

sity with  $f$ . Sharper Bragg peaks occur for the first time at  $f = 0.73$ . This  $f$  value corresponds to the vapor pressure  $p_a$  of the adsorption isotherm. Thus the structural data indicate, in agreement with the thermodynamic data, the onset of capillary condensation. It is the capillary condensed solid in the center of the pores and not the wall coating which is respon-

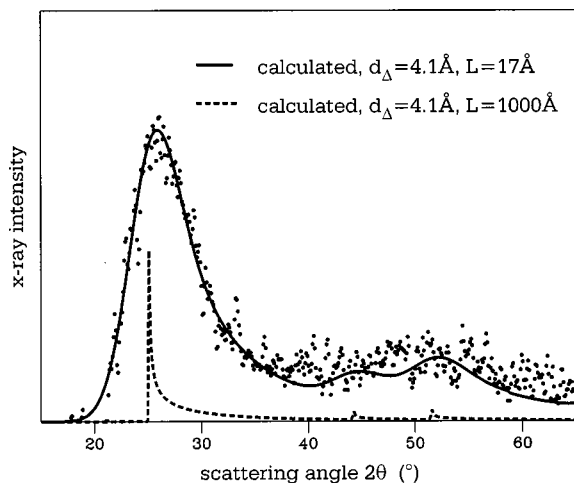


FIG. 5. Comparison of the measured monolayer diffraction pattern of N<sub>2</sub> ( $f = 0.11, D = 75 \text{ \AA}$ ) with powder patterns calculated for a two-dimensional triangular lattice.  $d_{\Delta}$  is the parameter of the triangular lattice,  $L$  its linear extension. The pattern for  $L = 1000 \text{ \AA}$  is shown on a reduced intensity scale.

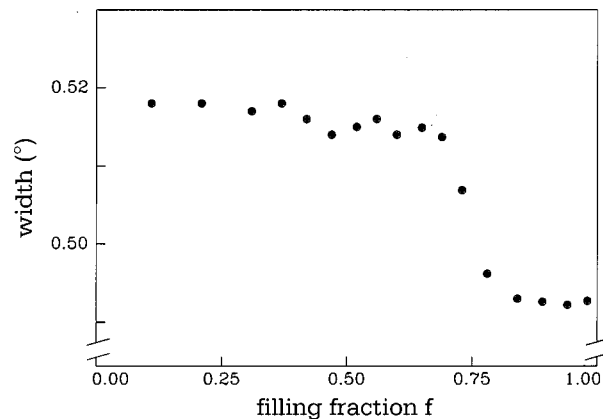


FIG. 6. The second moment of the first maximum of the diffraction patterns of Fig. 4 [which develops at higher  $f$  into the hcp reflections (100), (002), and (101)] as a function of the fractional filling  $f$ .

sible for the quasi-hcp component of the diffraction pattern. This is also documented in Fig. 6 which shows the  $f$  dependence of the width of the first maximum of the diffraction pattern. Clearly, there is a break at the onset of capillary condensation around  $f = 0.73$ . This  $f$  value corresponds to a thickness of wall coating of roughly four monolayers. For higher  $f$ , the patterns can be decomposed into the amorphous contribution of the adsorbate on the walls and the quasi-hcp capillary condensate, the amount of the latter part being given by  $f - 0.73$ . Analogous observations have been made for confined Ar,

### B. Carbon monoxide

All measurements on CO have been made for pores with  $D = 75 \text{ \AA}$ . Figure 7 shows the pattern of almost completely filled pores at three different temperatures and of the two phases of an evaporated bulk film for comparison. The diffraction pattern of the pore material at  $T = 65 \text{ K}$  (4 K below the triple point of bulk CO) is of the liquid type. At  $T = 55 \text{ K}$  the diffraction pattern is of the hcp type and similar to that of pore condensed N<sub>2</sub> (Fig. 2). On further cooling there is a substantial change to a pattern which is clearly of the  $Pa3$  type, known from the  $\alpha$  phase of the bulk solid. Thus confined CO, in contrast to N<sub>2</sub>, still undergoes the phase transition from the orientational disordered  $\beta$  phase with a hcp center-of-mass lattice to the orientational ordered  $\alpha$  phase with a fcc center-of-mass lattice. Further insight into the structural behavior of pore condensed CO on heating and cooling is obtained from Figs. 8 and 9. Figure 8 shows the evolution of the diffraction pattern, Fig. 9 the intensity of three selected reflections. The  $(100)_{\beta}$  reflection is a measure of the volume fraction of the quasi-hcp  $\beta$  phase;  $(200)_{\alpha}$  represents the material with a fcc center-of-mass lattice, independent of whether the CO-quadrupole moments have achieved the peculiar  $Pa3$ -type orientational ordering or not. The  $(210)_{\alpha}$  reflection, on the other hand, is related to just this structural pattern of orientational order. The square root of the  $(210)_{\alpha}$  intensity can be regarded as the orientational order parameter of the  $Pa3$  phase.

Hcp Bragg peaks appear on cooling at about 62 K; the capillary condensed component solidifies. It forms the quasi-

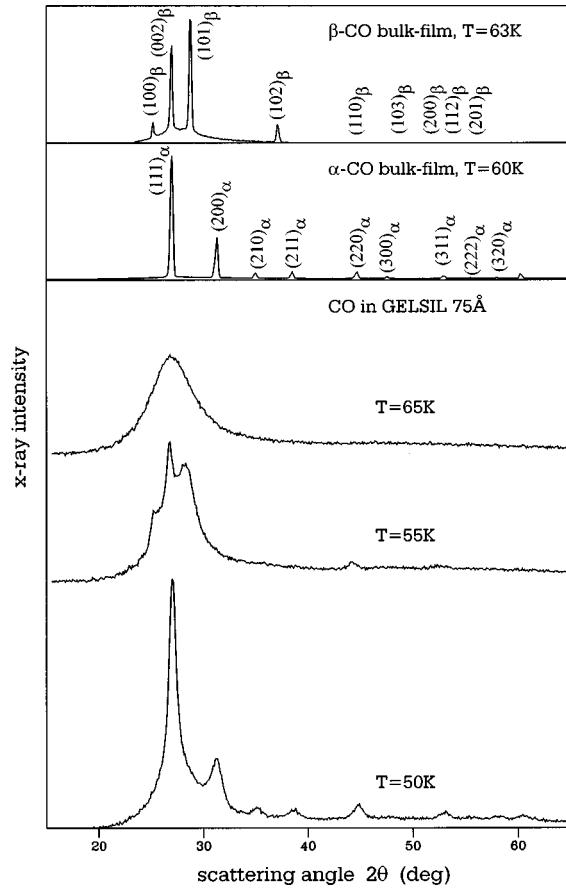


FIG. 7. Diffraction pattern of a bulk-film CO above (63 K) and below (60 K)  $T_{\alpha\beta}^{\text{bulk}}$  and of CO in 75 Å pores at three different temperatures, representing the liquid state and the  $\beta$  and  $\alpha$  phases of the pore condensate.

hcp  $\beta$  structure already known from  $\text{N}_2$ . In the temperature range from 54 to 52 K the reflections of the  $\beta$  and  $\alpha$  phases coexist. Below 52 K the hcp phase has disappeared and the material is in the  $\alpha$  phase. On heating there is a decrease of the  $Pa3$  specific reflections such as  $(210)_\alpha$  starting at about 54 K. Above 58 K these reflections are absent. However, the  $(200)_\alpha$  reflection can be observed up to significantly higher temperatures. On heating there is a  $T$  range, from about 58 to 61 K, in which the structure is fcc and not  $Pa3$ . Here the CO orientations are already disordered, but the center-of-mass lattice is still fcc. The fcc phase transforms back into the hcp  $\beta$  phase via a wide coexistence region. Around 63 K the pore condensed solid is in the single-phase  $\beta$  region. Melting occurs at about 64 K. Thus the phase sequence is liquid-hcp- $Pa3$  on cooling, but  $Pa3$ -fcc-hcp-liquid on heating. On heating out of the  $Pa3$  phase, the orientational disordering no longer coincides with the reconstruction of the stacking sequence of the center-of-mass lattice from fcc to hcp. Regions of phase coexistence have a typical breadth of 2 K, except for the fcc-to-hcp transition, which extends over 8 K. All phase changes show a thermal hysteresis between heating and cooling: the transition temperatures are reduced relative to the bulk state. The largest hysteresis, of about 8 K, is observed for the transformation of the center-of-mass lattice.

Additional information on the phase transitions comes from the temperature dependence of the molar volume  $V_m$  (Fig. 10), as determined from the lattice parameter of the

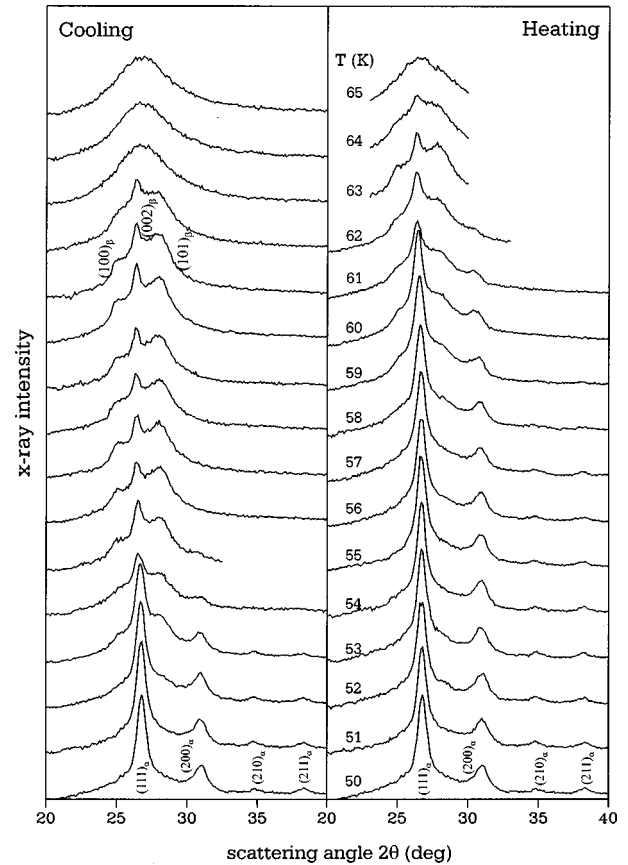


FIG. 8. The diffraction pattern of confined CO ( $D=75$  Å) as measured on cooling and heating. The temperatures given refer to the patterns of the left panel, too.

diffraction results. Figure 10 also includes data for the bulk solid. The change  $\Delta V$  of the volume at the transition has about the same value in the bulk and in the capillary condensed state. The volume jump of the pore condensate coincides with the hcp- $Pa3$  transition on cooling and with the  $Pa3$ -fcc transition on heating. Thus  $\Delta V$  is connected with the orientational order-disorder transition and not with the transformation of the center-of-mass lattice. The pore phases have larger volumes and are less dense than the corresponding bulk states. This is presumably due to a lot of lattice defects which the solid has to form in order to adapt to the pores. The difference with respect to the bulk is larger in the orientationally ordered low- $T$  phase than in the disordered high- $T$  phase. The relatively large value of  $V_m$  in the  $Pa3$  phase of the pore condensate is presumably connected via the orientation-strain coupling with a great deal of random orientational disorder, that is, with deviations of the orientations for the easy  $\langle 111 \rangle$  directions in particular in the neighborhood of lattice defects. On the other hand, the fcc center-of-mass lattice of the  $Pa3$  phase appears to be more perfect than the high- $T$  hcp phase. In the  $Pa3$  phase the stacking fault probability is only about 0.05 compared to 0.3 in the hcp phase.

In the following the thermodynamic state of the CO capillary condensate is characterized by the emptying pressure  $p_d(T)$ . The pressure is converted into the difference of the chemical potential with respect to the bulk system,  $\mu - \mu^{\text{bulk}} = k_B T \ln(p)$ : the resulting phase diagram is shown in

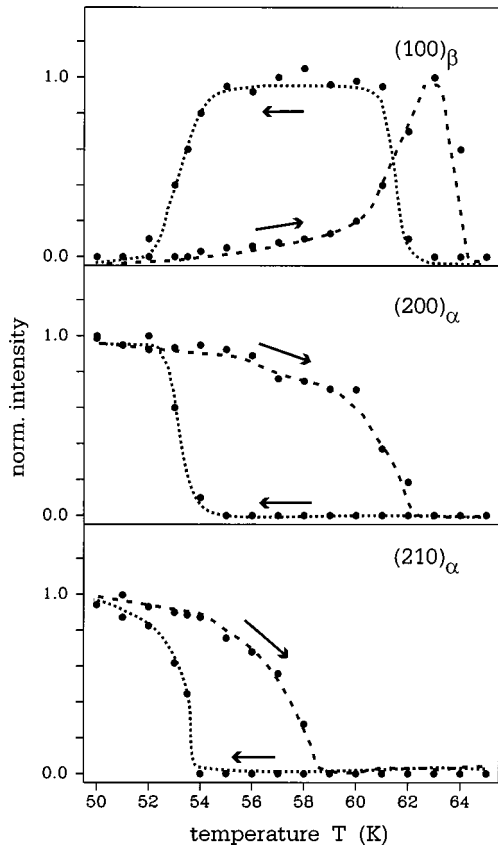


FIG. 9. The intensity of three reflections of CO in 75 Å pores as a function of temperature on cooling and heating.

Fig. 11. The chemical potential of the bulk liquid and its extrapolation to temperatures below  $T_3^{\text{bulk}}$  is used as a zero reference line. The data on the bulk condensate ( $p=1$ ) have been obtained by overfilling the pores with CO. The data on

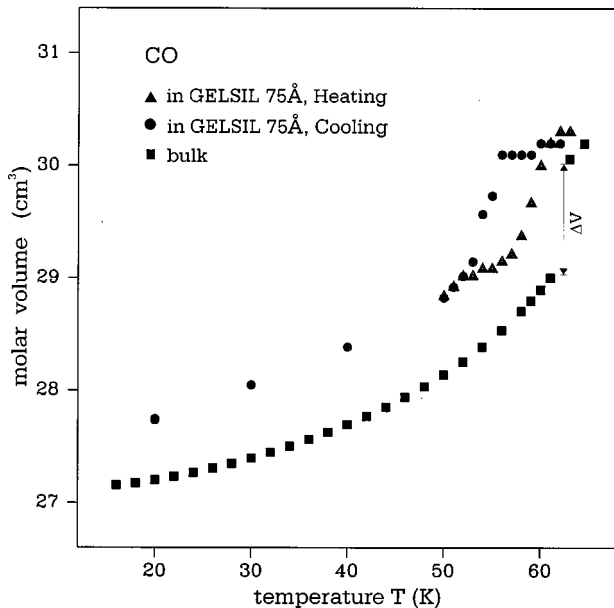


FIG. 10. The molar volume of bulk CO (solid line, from Refs. 19 and 20) and of CO confined in 75 Å pores as a function of temperature.

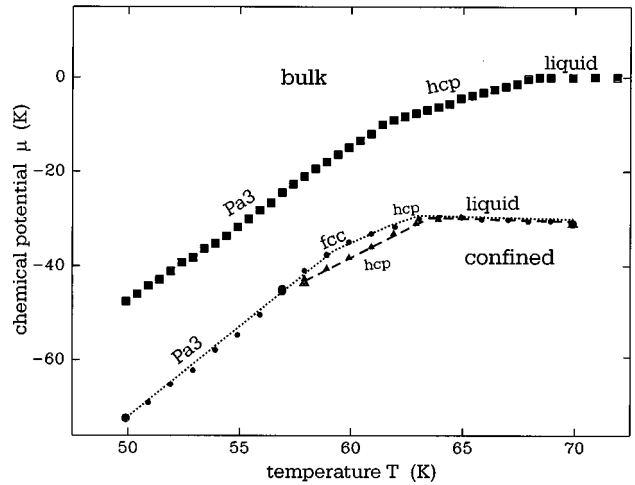


FIG. 11. The chemical potential of bulk CO (squares) and of capillary condensed CO ( $=\mu_d$ ) in 75 Å pores for different thermal histories: heating out of the  $\alpha$  phase along the fcc branch (circles), heating out of the  $\beta$  phase along the hcp branch (triangles). Large symbols refer to data points which have been determined from isotherms. The chemical potential of the bulk liquid is used as a zero reference line.

$\mu_d$  (related to  $p_d$ ) are from a few adsorption-desorption isotherms, which are of the same type as those shown for N<sub>2</sub> in Fig. 1, and from quasi-isosteric heating runs where the system is held in the steep part of the desorption branch of the isotherms.

The  $T$  variation of  $\mu^{\text{bulk}}$  is in agreement with the literature. The kinks at about 68 and 61.5 K define  $T_3^{\text{bulk}}$  and  $T_{\alpha\beta}$ . The entropy of melting and the entropy of the  $\alpha$ - $\beta$  transition as obtained from the difference of the slopes ( $S = -\partial\mu/\partial T$ ) above and below the corresponding phase transition temperature are  $(11.9 \pm 0.5)$  and  $(10.7 \pm 0.5)$  J/mol/K, in agreement with the literature (see Table I).

The  $\mu$ - $T$  diagram of Fig. 11 shows that capillary condensed CO has a smaller chemical potential than bulk CO, both in the liquid and solid phases. The difference  $\Delta\mu_d^i$  ( $i = \text{liquid}, \beta, \alpha$ ) of the chemical potential relative to the bulk system is larger in the liquid state than in the solid phases. The same observations have been made for Ar. The melting temperature  $T_m$  is indicated by the kink of  $\mu_d(T)$  at about 63 K. As pointed out in Ref. 5, the reduction of  $T_m$  relative to  $T_3^{\text{bulk}}$  is a consequence of the fact that  $\Delta\mu_d^{\text{liquid}} > \Delta\mu_d^\beta$ . In an analogous way the reduced phase transition temperature of the pore solid is given by  $T_{\alpha\beta} = T_{\alpha\beta}^{\text{bulk}} - (\Delta\mu_d^\beta - \Delta\mu_d^\alpha)/\Delta S_{\alpha\beta}$ . All  $\Delta\mu$ 's can be extracted from Fig. 11.

In the following we discuss the chemical potential  $\mu_d(T)$  of the capillary condensate in the solid state. Diffraction has shown that different phase sequences are obtained on heating and cooling. Since  $\mu_d(T)$  has to be measured on heating rather than on cooling, we have to use special routes in order to get into the competing mesophases fcc and hcp: The condensate is brought to low temperatures where it is in the Pa3 phase, and  $\mu_d(T)$  is recorded on subsequent heating (fcc branch of Fig. 11) along the sequence Pa3-fcc-hcp-liquid. The kink of  $\mu_d(T)$  at about 58 K marks the transition from the Pa3 phase into the orientationally

disordered fcc phase. The subsequent transformation of the center-of-mass lattice from fcc to hcp cannot be identified on the basis of the data on  $\mu_d(T)$ . In a second experiment the condensate is cooled down from the liquid state into the hcp phase at 58 K and  $\mu_d(T)$  is measured on subsequent heating (hcp branch). As shown in Fig. 11 the chemical potential of the hcp state of the hcp branch is lower than that of the fcc state of the other branch.

Finally, the solid mesophase has been formed by adsorption and brought to  $\mu_d$  by subsequent desorption at 58 K. The resulting value of  $\mu_d$  falls on the hcp branch of Fig. 11. The structure of the capillary condensate so prepared is in fact hcp, as has been verified by diffraction. Thus the stable configuration at intermediate temperatures is hcp and not fcc. The fcc configuration is a metastable or long-lived instable state. Note, however, that the difference of the chemical potential of the two configurations is minute and the entropies practically identical.

### C. Comments on the structural phase transition

The hcp- $Pa3$  transition is known from the bulk solids of  $N_2$ , CO, ortho- $H_2$ , and para- $D_2$ ; it involves the orientational ordering of the molecular quadrupole moments and the reconstruction of the center-of-mass lattice from the hcp  $AB\dots$  to the fcc  $ABC\dots$  stacking sequence. The understanding of this type of transition is incomplete because an order parameter in the sense of Landau theory cannot be formulated and because computer simulations cannot deal with changes of the stacking sequence within a reasonable computing time.<sup>21,22</sup> The theoretical and computational efforts rather treat the orientational ordering on the hcp and fcc center-of-mass lattices separately. The following results have been obtained from computer simulations:<sup>23,24</sup> The free energies of the disordered hcp and fcc phases are practically identical. On the fcc lattice, there is a transition into the  $Pa3$  phase. Here the directors of neighboring molecules form an angle of  $109^\circ$ , which is relatively close to the minimum ‘‘ $T$ ’’ configuration of a pair of molecules interacting via a quadrupole-quadrupole interaction. On the hcp lattice, however, this interaction is highly frustrated and only short-range orientational order develops at temperatures which are significantly lower, about 30%, than calculated fcc- $Pa3$  transition temperature. The short-range orientational arrangement is reminiscent of the pinwheel phase known from compressed CO monolayers adsorbed on graphite.<sup>25</sup> The formation of long-range orientational order is preempted by the freezing of the quadrupole moments in the local crystal field potential.

Indeed, the present results show that the chemical potentials of the hcp  $\beta$  phase and of the orientationally disordered fcc phase, which can be prepared by heating pore condensed CO out of the  $\alpha$  phase, are almost identical (Fig. 11) and that there are no anomalies of thermodynamic observables at the fcc-to-hcp transformation. This also means that the energy of a stacking fault is small and that accordingly the stacking fault probability in the orientationally disordered fcc and hcp mesophases is large. The transition from hcp to  $Pa3$  on cooling is triggered by the orientation-dependent intermolecular interactions; the stacking sequence of the center-of-mass lattice is changed from hcp to fcc mainly in order to

satisfy the orientation-dependent, quadrupolar interactions. The orientational ordering lifts the previous degeneracy of the fcc and hcp stacking sequences in the orientationally disordered state and establishes the fcc stacking sequence of the  $Pa3$  structure, thereby eliminating most of the stacking faults of the high- $T$  phase. Clearly, a certain number of lattice defects is necessary for the accommodation of the crystalline solid to the pore geometry, but lattice defects are definitely more costly in the orientationally ordered phase than in the disordered phase. Presumably, this is the reason why the difference of the chemical potential between the pore solid and bulk solid is smaller in the ordered than in the disordered state,  $\Delta\mu^\alpha < \Delta\mu^\beta$ , with the consequence that  $T_{\alpha\beta}$  is lower than in the bulk.

The peculiar behavior of CO gives access to the quadrupolar order-disorder transition on a fcc center-of-mass lattice, the  $(210)_\alpha$  intensity being related to the order parameter. Landau theory calls for a phase transition of first order.<sup>21</sup> The experiment on the pore condensed material (Figs. 8 and 9) rather suggests a continuous decrease of the peak intensity, which of course may be due to different transition temperatures in pore sections with different diameters.

Why is the hcp- $Pa3$  transition suppressed in pore condensed  $N_2$ , but not in CO? fcc-hcp transformations are known from solid He and from several metals like Co. The highly cooperative ‘‘martensitic’’ mechanism of such transformations results from the principle of the minimization of strain energy. The smallest stack of close-packed planes, fcc (111) or hcp (001), which can be inserted coherently into the lattice of the other kind, contains just six layers.<sup>26,27</sup> In crystallites smaller than that or in samples which contain lattice defects, some uncompensated transformation strain will appear. The fcc-hcp transformation will only take place if the difference of volume free energy can account for this strain energy. This situation obviously occurs in pore condensed CO, but cannot be accomplished in pore condensed  $N_2$ . For  $N_2$  the orientation-dependent contribution to the volume free energy of the ordered phase is smaller because of the smaller quadrupole moment, while on the other hand the strain energies, which depend in the first respect on the isotropic part of the intermolecular interactions, are little different from those in CO. From this reasoning one expects a downward shift of the hcp-to- $Pa3$  transformation temperature which is larger for  $N_2$  than for CO. If the transformation is delayed to such an extent that the thermal energy becomes small compared to the barriers for reorientation, the hcp- $Pa3$  transition will no longer take place. Considering the fact that  $T_{\alpha\beta}$  is *a priori* lower for  $N_2$  than for CO and that the barriers are presumably comparable, the different structural behavior of the two pore condensates is plausible.

Thus pore condensed  $N_2$  remains hcp down to lowest temperatures, even in pores as wide as  $130 \text{ \AA}$ . As far as the stability of the pore condensed hcp phase of  $N_2$  is concerned, one can estimate the temperature at which the chemical potential of the bulk  $Pa3$  phase is equal to the chemical potential of capillary condensed hcp  $N_2$  by extrapolating  $\mu^{\text{bulk}}(T)$  and  $\mu_d(T)$  to low  $T$ . One arrives at values around 0 K. Thus the hcp pore filling appears to be stable with respect to a transformation into bulk  $Pa3$  material, even if it would remain in a state of dynamic orientational disorder at low  $T$ . Thus one can exclude a dewetting transition. Does the  $N_2$

hcp pore material undergo any structural change on cooling? There are no superlattice peaks at low  $T$  which would indicate long-range orientational order. At low  $T$ , thermally activated reorientations come necessarily to rest: the quadrupole moments freeze in and form an “orientational glass.” The experiment gives no information on the structure of the local orientational patterns and on the size of the coherent regions.

Finally, it should be noted that a structural behavior analogous to that found in the pore condensates of CO and N<sub>2</sub> has been observed in mixed crystals when the quadrupolar species N<sub>2</sub>, ortho-H<sub>2</sub>, or para-D<sub>2</sub> is diluted by suitable substitutional spherical molecules (Ar, para-H<sub>2</sub>, and ortho-D<sub>2</sub>, respectively).<sup>28,29</sup> Detailed information exists for (N<sub>2</sub>)<sub>x</sub>Ar<sub>1-x</sub>. For such mixed crystals with  $x$  around 0.9, a sequence of phases has been observed on cooling and heating<sup>30</sup> which is identical to that of pore condensed CO. For mixed crystals with  $x < 0.8$ , the  $\alpha$ - $\beta$  transition is completely suppressed<sup>29</sup> in a way analogous to the situation in pore condensed N<sub>2</sub>. Obviously, the confinement in pores and substitutional defects have similar effects on the structural behavior of N<sub>2</sub> and CO.

#### IV. CONCLUSIONS

The present experiment has given information on the thermodynamic and structural state of N<sub>2</sub> and CO solidified in a nanoporous SiO<sub>2</sub> matrix. For any fractional filling  $f$ , the pore condensate is stable with respect to the bulk condensates outside the pores. The pore condensate profits from the attractive potential of the pore walls. We have no indication for a dewetting transition, a process which has been discussed for pore condensed H<sub>2</sub>.<sup>11,31</sup> At low filling the pore condensate exists as adsorbate on the pore walls: at higher filling the pore center is filled via capillary condensation, which is a phase transition of first order. The critical thickness of the adsorbate where this occurs depends on temperature and pore diameter. The chemical potential of the capil-

lary condensate is only slightly lower than that of the bulk material. A typical difference  $\Delta\mu$  is 30 K. The difference is somewhat larger in the liquid state than in the solid state with the consequence that the melting temperature is lower than in the bulk. The adsorbate on the pore walls is amorphous, remotely related to a two-dimensional triangular lattice with a coherence length of about four intermolecular distances. The structure of the solidified capillary condensate in the center of the pores is similar to that of the bulk solid, but contains a lot of lattice defects, stacking faults in particular, which are obviously the price the pore solid has to pay for the accommodation to the confined geometry. The coherence length of the crystallized material in the pore center exceeds the pore diameter. As far as these fundamental thermodynamic and structural properties are concerned, N<sub>2</sub> and CO behave in a way analogous to Ar.

At lower temperatures capillary condensed CO and N<sub>2</sub> behave differently. N<sub>2</sub> remains in the quasi-hcp state down to lowest temperatures without any indication of long-range quadrupolar ordering. CO transforms into the ordered  $Pa3$  structure known as the low- $T$  phase of the bulk solids. On heating a quadrupolar order-disorder transition brings the system into an intermediate orientationally disordered fcc phase, unknown in bulk CO. The high- $T$  phase is restored by a martensitic fcc-hcp transition. The structural transition temperature of CO is lower than in the bulk. This is due to the fact that the orientationally disordered “plastic” phase can adapt to the confinement more easily than the orientationally ordered phase. The different structural behavior of pore condensed N<sub>2</sub> and CO results from different ratios of the isotropic and of the anisotropic part of the intermolecular interactions.

#### ACKNOWLEDGMENT

This work has been supported by the Sonderforschungsbereich 277 “Grenzflächenbestimmte Materialien.”

- <sup>1</sup>M. H. W. Chan, K. I. Blum, S. Q. Murphy, G. K. S. Wong, and J. D. Reppy, *Phys. Rev. Lett.* **61**, 1950 (1988).
- <sup>2</sup>E. Molz, A. P. Y. Wong, M. H. W. Chan, and J. R. Beamish, *Phys. Rev. B* **48**, 5741 (1993).
- <sup>3</sup>M. W. Cole and W. F. Saam, *Phys. Rev. Lett.* **32**, 985 (1974).
- <sup>4</sup>R. Evans, U. M. B. Marconi, and P. Tarazona, *J. Chem. Soc., Faraday Trans. 2* **82**, 1763 (1986).
- <sup>5</sup>P. Huber and K. Knorr, preceding paper, *Phys. Rev. B* **60**, 12 657 (1999).
- <sup>6</sup>T. A. Scott, *Phys. Rep.* **3**, 85 (1976).
- <sup>7</sup>N. G. Parsonage and L. A. K. Staveley, *Disorder in Crystals* (Clarendon, Oxford, 1978).
- <sup>8</sup>P. Huber, D. Wallacher, and K. Knorr, *J. Low Temp. Phys.* **111**, 419 (1998).
- <sup>9</sup>D. Wallacher, P. Huber, and K. Knorr, *J. Low Temp. Phys.* **113**, 823 (1998).
- <sup>10</sup>P. I. Ravikovitch, S. C. Ó. Domhnaill, A. V. Neimark, F. Schüth, and K. K. Unger, *Langmuir* **11**, 4765 (1995).
- <sup>11</sup>P. E. Sokol, R. T. Azuah, M. R. Gibbs, and S. M. Bennington, *J. Low Temp. Phys.* **103**, 23 (1996).
- <sup>12</sup>Y. Wang, W. M. Snow, and P. E. Sokol, *J. Low Temp. Phys.* **101**, 929 (1995).
- <sup>13</sup>J. Warnock and D. D. Awschalom, *Phys. Rev. B* **35**, 1962 (1987).
- <sup>14</sup>C. L. Jackson and G. B. McKenna, *J. Chem. Phys.* **93**, 9002 (1990).
- <sup>15</sup>K. M. Unruh, T. E. Huber, and C. A. Huber, *Phys. Rev. B* **48**, 9021 (1993).
- <sup>16</sup>M. W. Maddox and K. E. Gubbins, *J. Chem. Phys.* **107**, 9659 (1997).
- <sup>17</sup>D. Marx and H. Wiechert, *Adv. Chem. Phys.* **95**, 213 (1996).
- <sup>18</sup>T. E. Huber and H. L. Tsou, *Phys. Rev. B* **57**, 4991 (1998).
- <sup>19</sup>I. N. Krupskii, A. I. Prokhvatilov, Y. A. Freiman, and A. I. Ernenburg, *Sov. J. Low Temp. Phys.* **5**, 130 (1979).
- <sup>20</sup>L. Vegard, *Z. Phys.* **88**, 239 (1934).
- <sup>21</sup>J. R. Cullen, D. Mukamel, S. Shtrikman, L. C. Levitt, and E. Callen, *Solid State Commun.* **10**, 195 (1972).
- <sup>22</sup>H. M. James and J. C. Raich, *Phys. Rev.* **162**, 649 (1967).
- <sup>23</sup>B. Kuchta, K. Rohleder, R. D. Eppers, and J. Belak, *J. Chem. Phys.* **102**, 3349 (1995).

- <sup>24</sup>S. Rauegi, G. Cardini, V. Schettino, and H. J. Jodl, *J. Chem. Phys.* **106**, 8196 (1997).
- <sup>25</sup>H. You and S. C. Fain, Jr., *Surf. Sci.* **151**, 361 (1985).
- <sup>26</sup>K. A. Mc Greer, K. R. Lundgren, and J. P. Franck, *Phys. Rev. B* **42**, 87 (1990).
- <sup>27</sup>O. Blaschko, G. Krexner, J. Pleschiutchnig, G. Ernst, C. Hitzemberger, H. P. Karnthaler, and A. Korner, *Phys. Rev. Lett.* **60**, 2800 (1988).
- <sup>28</sup>A. F. Schuch, R. L. Mills, and D. A. Depatie, *Phys. Rev.* **165**, 1032 (1968).
- <sup>29</sup>H. Klee, H. O. Carmesin, and K. Knorr, *Phys. Rev. Lett.* **61**, 1855 (1988).
- <sup>30</sup>H. Klee and K. Knorr, *Phys. Rev. B* **43**, 8658 (1991).
- <sup>31</sup>M. Schindler, A. Dertinger, Y. Kondo, and F. Pobell, *Phys. Rev. B* **53**, 11 451 (1996).